

1 Oxygenation of the Archean atmosphere: New paleosol constraints from
2 Eastern India

3
4 Joydip Mukhopadhyay^{1,3}, Quentin G. Crowley^{2#}, Sampa Ghosh¹, Gautam Ghosh¹, Kalyan
5 Chakrabarti^{1,4}, B. Misra^{1,4}, Kyle Heron² and Sankar Bose¹

6 ¹*Department of Geology, Presidency University, Kolkata, India,*

7 ²*Department of Geology, School of Natural Sciences, Trinity College Dublin, Ireland*

8 ³*PPM Research Group, Department of Geology, University of Johannesburg, Johannesburg*

9 ⁴*Atomic Minerals Directorate, Eastern Region, Jamshedpur, India*

10 *#Communicating author: E-mail: crowleyq@tcd.ie*

11
12 **ABSTRACT**

13 **It is widely believed that atmospheric oxygen saturation rose from $<10^{-5}$ Present**
14 **Atmospheric Level (PAL) in the Archean to $>10^{-2}$ PAL at the Great Oxidation Event**
15 **(GOE) around 2.4 billion years ago, but it is unclear if any earlier oxygenation events**
16 **occurred. Here we report U-Pb zircon data indicating a pyrophyllite-bearing paleosol,**
17 **from Keonjhar in the Precambrian Singhbhum Craton of eastern India, formed**
18 **between 3.29 and 3.02 billion years ago, making it one of very few known Archean**
19 **paleosols globally. Field and geochemical evidence suggests that the upper part of the**
20 **paleosol was eroded prior to unconformable deposition of an overlying sequence of**
21 **shallow-marine siliciclastic sediments. A negative cerium anomaly within the currently**
22 **preserved level of the paleosol indicates that ancient oxidative weathering occurred in**
23 **the original upper soil profile. The presence of redox sensitive detrital uraninite and**
24 **pyrite together with a complete absence of pyrophyllite in the overlying sediments**
25 **indicate that the mineralogical and geochemical features of the paleosol were**

26 established prior to unconformable deposition of the sediments and are not related to
27 subsequent diagenetic or hydrothermal effects. We suggest a transient atmospheric
28 oxygenation event occurred at least 600 million years prior to the GOE and
29 approximately 60 million years prior to a previously documented Archean oxygenation
30 event. We propose that several pulsed and short-lived oxygenation events are likely to
31 have occurred prior to the GOE and that these changes to atmospheric composition
32 arose due to the presence of organisms capable of oxygenic photosynthesis.

33

34 **Key Words:** Paleosol; atmospheric oxygen; Archean; detrital zircon; Singhbhum Craton

35 INTRODUCTION

36 Paleosols are ancient soil horizons formed by terrestrial weathering of rock surfaces.
37 They preserve chemical records of atmospheric composition and various biotic or abiotic
38 mediated chemical weathering pathways at the time of their formation. Paleosols from “deep
39 time” provide a valuable opportunity to study evolution of the early atmosphere and
40 emergence of distinct processes on Earth (Bekker et al., 2004; Holland, 2006). Very few
41 Archean paleosols have been documented worldwide; these include the Pilbara (Johnson et
42 al., 2008; 3.4 billion years (Ga) old), Nsuze (Crowe et al., 2013; c. 2.96 Ga) and Mt Roe
43 (Macfarlane et al., 1994; 2.76 Ga) paleosols. The Pilbara and Mt. Roe paleosols, both of
44 which occur in Pilbara NW Australia, indicate surface weathering took place in an oxygen
45 poor atmosphere (Macfarlane et al., 1994; Yang et al., 2002), although controversy exists
46 surrounding the Mt Roe Paleosols in that some studies suggest oxygen was present (Ohmoto,
47 1996; Phillippot et al., 2013). Recent work on the Nsuze Paleosol (Crowe et al., 2013) from
48 the Pongola Supergroup of South Africa suggests that by 2.96 Ga oxygen levels had risen to
49 at least 3×10^{-4} PAL, thus extending the chemical record of the first appreciable levels of
50 atmospheric oxygen by about 500 million years.

51 Here we describe a previously undated supra-crustal sequence in the Singhbhum Craton
52 of eastern India. We demonstrate that a paleosol, termed the Keonjhar Paleosol, formed
53 between 3.29 and 3.02 Ga and did so in the presence of molecular oxygen. This is the world’s
54 oldest documented example of oxidative weathering. These findings further push back the
55 age at which a pre-GOE oxygenation of the Earth’s atmosphere occurred. By integrating our
56 findings with those from Archean supra-crustal rocks, we give additional support to proposed
57 models for both a pre-GOE oxygenation (Anbar, 2007; Crowe et al., 2013; Planavsky et al.,
58 2014) and fluctuating Archean atmospheric oxygen levels (Lyons et al., 2014; Rosing & Frei,
59 2004).

60

61 **GEOLOGICAL SETTING**

62 The Keonjhar Paleosol has previously been described; however there have been no
63 radiometric age constraints on its formation and it was speculated to be Palaeoproterozoic in
64 age (Bandopadhyay et al., 2010). The paleosol occurs between a Paleo- to Mesoarchean (3.3
65 to 3.1 Ga) multi-component tonalite-trondhjemite-grandiorite (TTG) batholith known as the
66 Singhbhum Granite and a thick unconformable succession of shallow-marine quartzarenite
67 sandstones and interbedded conglomerates (Fig. 1A). These siliciclastic sediments are exposed
68 along a near continuous outcrop bordering a Paleoarchean (3.51 to 3.3 Ga) greenstone belt
69 termed the Iron Ore Group (Mukhopadhyay et al., 2008; Mukhopadhyay et al., 2012). The
70 quartzarenite sandstones are known as the Mahagiri Quartzite in the southeast and the Pal
71 Lahara-Mankaharchua Quartzite in the west, along a southeast-northwest transect of over 100
72 km from the town of Keonjhar (Fig. 1A). One part of the sandstone outcrop also extends
73 north for over 80 km from Keonjhar. A clear angular unconformity exists between the
74 sandstones and underlying greenstone belt rocks as well as the TTG granitoids
75 (Mukhopadhyay et al., 2012). The best exposures of Keonjhar Paleosol occur around
76 Madrangijori village, 6 km north of Keonjhar (Fig. 1A). Here quartzarenite sandstones can be
77 observed unconformably overlying the paleosol (Fig. 1B), which passes downwards into
78 altered granite. The paleosol thickness varies from one metre to more than six metres and is
79 distinguished by its contrasting pale colour and talc-like feel. Petrographically the paleosol is
80 dominantly composed of pyrophyllite and quartz (Fig. 1C), with subordinate amounts of illite
81 and muscovite. Pyrophyllite formed from kaolinite and quartz in very low grade metamorphic
82 conditions, whereas kaolinite formed due to chemical weathering of feldspar from the original
83 granite. Pyrophyllite does not occur in the overlying sediments; therefore the chemical
84 weathering which originally resulted in formation of the paleosol predates deposition of the

85 unconformably overlying sediments. The siliciclastics from this region contain detrital
86 uraninite and pyrite (Fig. 1D, E), which have also previously been described from quartz
87 pebble conglomerates near the western margin of the Bonai Granite (Fig. 1) (Kumar et al.,
88 2012). The presence of detrital uraninite and pyrite is significant in that they illustrate surface
89 oxygen conditions did not exceed 10^{-3} PAL (Canfield et al., 2000) at the time of their
90 deposition.

91

92 **AGE OF THE KEONJHAR PALEOSOL**

93 A component of the Singhbhum Granite, termed the Keonjhara-Bhaunra Granite, forms the
94 “basement” to the paleosol. It has been dated at c. 3.29 Ga (Tait et al., 2011) and represents
95 the oldest possible age of formation of the Keonjhar Paleosol. Here we present U-Pb detrital
96 zircon age spectra from seven representative samples (Table DR1) of the entire quartzarenite
97 sandstone outcrop belt. Our samples cover an extensive geographic area (Fig. 1), so constitute
98 representative detrital zircon populations to limit the sedimentation age of the sandstones and
99 provide an upper age bracket for the formation of the Keonjhar Paleosol. U-Pb detrital zircon
100 ages from seven samples and 431 out of 770 analyses which are less than 10% discordant
101 reveal detrital zircons between c. 3.58 and 3.02 Ga (Fig. 2A). The youngest detrital zircon
102 population (3.02 Ga) was derived from a source significantly younger than the underlying
103 granite. Overall, detrital zircon data indicate sandstones formed by recycling of several
104 sources of pre-existing zircon-bearing differentiated crust. It is not possible to accurately
105 estimate the time span between formation of the Keonjhar Paleosol and a change in relative
106 sea level which resulted in unconformable deposition of the overlying siliciclastic sediments.
107 The Keonjhar Paleosol is therefore conservatively constrained as having formed between
108 crystallisation of the Keonjhara-Bhaunra Granite and the youngest detrital zircon population
109 in the overlying sandstones; between 3.29 and 3.02 Ga. Consideration is also given to the

110 possibility that the sediments may be considerably younger than suggested by the youngest
111 detrital zircons. The presence of redox-sensitive detrital pyrite and uraninite in these
112 sediments signifies pre-GOE deposition which could potentially be compatible with an
113 earliest Paleoproterozoic age. Other stratigraphic units now preserved in different parts of the
114 Singhbhum Craton (e.g. Dhanjori, Singhbhum and Kolhan Groups) contain abundant detrital
115 zircons ranging from Neoproterozoic to Paleoproterozoic or Mesoproterozoic in age (Acharyya
116 et al., 2010 and our unpublished U-Pb detrital zircon data from the Kolhan Group). In this
117 respect, the absence of Proterozoic detrital zircons from the siliciclastic sediments
118 immediately overlying the Keonjhar Paleosol is a direct consequence of their Archean
119 depositional age and is not an artefact of the restricted availability of younger zircons in the
120 supracrustals of this region. Additionally, we have observed 2.8 Ga granitoids (Misra et al.,
121 2000) intruding Mahagiri Range quartzarenites (DT area in Fig. 1A), thus giving a minimum
122 2.8 Ga age to this entire Archean supra-crustal succession. This unequivocally places the
123 Keonjhar Paleosol as amongst the oldest known such example on Earth, having formed
124 sometime between the Pilbara and Nusze paleosols.

125

126 **GEOCHEMISTRY OF THE PALEOSOL**

127 Major, trace and Rare Earth Element (REE) compositions Keonjhar Paleosol samples
128 devoid of surficial weathering have been determined (Table DR2). In order to characterize
129 the alteration profile molar ratios of (i) immobile, (ii) redox sensitive and (iii) mobile
130 elements are plotted relative to Ti (Fig. 2B), as the latter is considered relatively immobile
131 during weathering. Exposures of unaltered “basement” granite were not observed in paleosol
132 sample locations, so for comparative purposes nearby fresh Keonjhar-Bhaunra Granite (Fig.
133 1) compositions (Tait et al., 2011) have been selected to assess chemical alteration with
134 respect to representative paleosol protolith compositions. Paleosol immobile element ratios

135 (e.g. Al/Ti, Nb/Ti, Ga/Ti and Y/Ti) are generally within ranges shown by the granite,
136 indicating the paleosol is *in situ*. A decrease in Th/Ti paleosol values suggests mobility of Th
137 and likely involvement of acidic fluids during pedogenesis (Langmuir, 1997). Redox
138 sensitive element ratios such as Fe_T/Ti and Mn/Ti are lower in the paleosol profile, whereas
139 V/Ti is generally higher relative to the granite, suggesting an original reducing soil
140 environment at these sampled depths. Mobile element concentrations relative to Ti (e.g.
141 Ca/Ti, Na/Ti, Cs/Ti, Mg/Ti, Ni/Ti and Zn/Ti) show a marked depletion from the granite
142 protolith to the paleosol, characteristic of leached weathering profiles, particularly in humid
143 climates. K/Ti, Rb/Ti and A-CN-K plots of two samples show alkali element enrichment
144 which may have occurred during K-metasomatism, but overall this is a minor geochemical
145 feature which has not affected the other analyzed samples.

146 Chondrite normalized paleosol REE profiles show negative Ce and Eu anomalies.
147 When normalized to the “basement” granite significant fractionation of paleosol REE is
148 evident (Fig. 2C). Heavy (H) REE are several orders of magnitude enriched compared to light
149 (L) REE; this may occur following intensive chemical weathering (Yusoff et al., 2013),
150 especially when organic-rich topsoil exists (Nesbitt, 1977). Organic-rich soil waters at
151 lowered pH are particularly aggressive in removing REE (Nesbitt & Marcovics, 1997).
152 Estimates of Archean atmospheric CO₂ concentration are 10¹ PAL, which may have resulted
153 in a rainwater pH of c. 4.6 (Ohmoto et al., 2004). Incipiently and moderately altered rocks are
154 known to be particularly enriched in HREE in alteration zones from lower parts of soil
155 profiles, while extremely altered residual products in upper parts are commonly depleted in
156 HREE (Nesbitt, 1977; Yusoff et al., 2013; Berger et al., 2014). Preferential HREE
157 enrichment in the preserved portion of the Keonjhar Paleosol profile, as well as lower Fe_T/Ti
158 and Mn/Ti and higher V/Ti with respect to the granite protolith therefore indicate the
159 preserved level of the paleosol most likely represents the lower part of the original soil profile

160 and alteration zone. Significantly, all paleosol samples show true negative Ce anomalies,
161 calculated as chondrite normalized $Ce/Ce^*-Pr/Pr^*$ (Fig. 2C). The presence of a negative Ce-
162 anomaly and HREE enrichment in the Keonjhar Paleosol suggest development of a zoned
163 soil profile analogous to modern tropical “lateritic” profiles with distinct wet and dry seasons
164 (Fitzpatrick, 1986). In lateritic soil profiles the upper part is oxidized where Mn and Fe oxy-
165 hydroxides accumulate as a Fe-Mn duricrust (Duzgoren-Aydin & Aydin, 2009). The pallid
166 zone immediately below the duricrust bears signatures of a reducing environment from which
167 soluble Fe^{2+} and Mn^{2+} migrate and precipitate at the top oxidized part during dry seasons
168 (Beukes et al., 2002). Negative Ce anomalies may form in regions of the soil profile where
169 REE except Ce have accumulated from an overlying oxidized zone. This occurs when Ce^{3+} is
170 transformed to the highly immobile Ce^{4+} , possibly involving cerianite ($Ce^{(IV)}O_2$)
171 precipitation, so that Ce retained in the upper soil profile and fractionated with respect to
172 trivalent REE (Berger et al., 2014). In this way, Ce is preferentially retained with Mn and Fe
173 oxy-hydroxides in a lateritic duricrust. The Keonjhar Paleosol now preserved below the
174 sandstone likely represents the pallid alteration zone of the lower part of a “lateritic” soil
175 profile marked by the characteristic Fe, Mn depletion, HREE enrichment and a negative Ce-
176 anomaly.

177 It is highly significant that siliciclastic sediments unconformably overlying the
178 paleosol do not demonstrate any mineralogical evidence for Fe-Mn enrichment. Furthermore,
179 there is no silicification, albitization or enrichment of diagnostic elements (e.g. Zn, Cu, W,
180 Sn, Mo) to support hydrothermal fluid passage along the granite-sandstone unconformity.
181 The described mineralogical and geochemical features of the Keonjhar Paleosol therefore
182 formed during a period of chemical weathering when the granite surface was exposed to the
183 atmosphere and that this occurred prior to deposition of the overlying siliciclastic sequence.

184

185 **CONCLUSIONS**

186 The presence of both oxidative weathering in the Keonjhar Paleosol and the presence
187 of redox sensitive minerals in the overlying quartzarenite may either signify a decrease in
188 atmospheric oxygen between paleosol formation and deposition of the overlying siliciclastics,
189 or alternatively that atmospheric oxygen was sustained at a relatively narrow concentration
190 interval (between c. 10^{-4} and 10^{-3} PAL) capable of sustaining both these features. Formation
191 of the Keonjhar Paleosol signifies the presence of molecular oxygen at levels above those
192 which could have been produced by photo-dissociation of atmospheric water alone (Kasting
193 and Walker, 1981). We propose this early, transient atmospheric oxygenation was due the
194 existence of micro-organisms capable of oxygenic photosynthesis. This is dramatically earlier
195 than most previous estimates for the development of photosynthesis (Des Marais, 2000;
196 Farquhar et al., 2011), but is not inconsistent with its development as a metabolic process
197 prior to the evolution of an entire genome for a photosynthetic organism (Xiong et al., 2000).

198 Previous attempts to compile chemical and isotopic data from Archean paleosols have
199 been limited by the small number of definite paleosols known from early Earth history (Rye
200 and Holland, 1998). Our study of the Keonjhar Paleosol highlights the importance of new
201 discoveries of such horizons in constraining atmospheric evolution at a higher temporal
202 resolution. These rare examples of paleosols from deep time provide the potential to link
203 geological, biological and environmental evidence to build a more comprehensive
204 understanding of secular changes in the early Earth System.

205

206 **ACKNOWLEDGEMENTS**

207 This work is supported by research funding from BRNS-India to JM and GG, a DST-India (SR/WOS-A/ES-
208 10/2010) grant to SG and a Trinity College Dublin (TCD) FEMS project fund to QGC, JM and GG. Thanks to
209 Balz Kamber for his generous support in providing additional analytical time at TCD for U-Pb zircon analyses.
210 This work forms part of PhD research by of KC and BM. JM, GG and SB acknowledge FRPDF grant from

211 Presidency University and a CSIR Research grant. UGC-CAS and DST-FIST laboratory facilities at Presidency
212 University have been used. JM, GG and QGC acknowledge logistic support provided by Tata Steel during
213 fieldwork. JM dedicates his contribution in memory of his teacher the Late Professor Asru Kumar Chaudhuri.

214

215 **REFERENCES CITED**

216 Acharyya, S. K., Gupta, A., and Orihashi, Y., 2010, Neoproterozoic–Paleoproterozoic stratigraphy of the
217 Dhanjori basin, Singhbhum Craton, Eastern India: And recording of a few U–Pb zircon dates
218 from its basal part: *Journal of Asian Earth Sciences*, v. 39, p. 527-536.

219 Anbar, A.D., Duan, Y., Lyons, T.W., Arnold, G.L., Kendall, B., Creaser, R.A., Kaufman, A.J.,
220 Gordon, G.W., Scott, C., Garvin, J., and Buick, R., 2007, A whiff of oxygen before the great
221 oxidation event?: *Science*, v. 317, p. 1903-1906.

222 Bandopadhyay, P.C., Eriksson, P.G., and Roberts, R.J., 2010, A vertic paleosol at the Archean-
223 Proterozoic contact from the Singhbhum-Orissa craton, Eastern India: *Precambrian Research*,
224 v. 177, p. 277-290.

225 Berger, A., Janots, E., Gnos, E., Frei, R., and Bernier, F., 2014, Rare earth element mineralogy and
226 geochemistry in a laterite profile from Madagascar: *Applied Geochemistry*, v. 41, p. 218-228.

227 Bekker, A., Holland, H.D., Wang, P.L., Rumble, D., Stein, H.J., Hannah, J.L., Coetzee, L.L., and
228 Beukes, N.J., 2004, Dating the rise of atmospheric oxygen: *Nature*, v. 427, p. 117–120.

229 Beukes N.J., Dorland, H., Gutzmer, J.G., Nedachi, M., and Ohmoto, H., 2002, Tropical laterites, life
230 on land, and the history of atmospheric oxygen in the Paleoproterozoic: *Geology*, v. 30, p.
231 491–494.

232 Canfield, D.E., Habicht, K.S., and Thamdrup, B., 2000, The Archean sulfur cycle and the early
233 history of atmospheric oxygen: *Science*, v. 288, p. 658–661.

234 Crowe, S.A., Døssing, L.N., Beukes, N.J. Bau, M., Kruger, S.J., Frei, R., and Canfield, D. E., 2013.
235 Atmospheric oxygenation three billion years ago: *Nature*, v. 501, p. 535-539.

236 Des Marais, D.J., 2000, When did photosynthesis emerge on Earth?: *Science*, v. 289, p. 1703-1705.

237 Duzgoren-Aydin, N.S., and Aydin, A., 2009, Distribution of rare earth elements and oxyhydroxide
238 phases within a weathered felsic igneous profile in Hong Kong: *Journal of Asian Earth*
239 *Sciences*, 34, p. 1-9.

240 Farquhar, J., Bao, H., and Thiemens, M., 2000, Atmospheric influence of Earth's earliest sulfur cycle:
241 *Science*, 289, p. 756-758.

242 Fitzpatrick, E.A., 1986, *An introduction to soil science*: Longman Scientific and Technical, Essex,
243 255 p.

244 Holland, H.D., 2006, The oxygenation of the atmosphere and oceans: *Philosophical Transactions of*
245 *the Royal Society of London*, ser. B, v. 361, p. 903–915.

246 Johnson, I.J., Watanabe, Y., Yamaguchi, K., Hamasaki, H., and Ohmoto, H., 2008, Discovery of the
247 oldest (~3.4 Ga) lateritic paleosols in the Pilbara Craton Western Australia: *Geological*
248 *Society of America Abstracts with Programs*, v. 40, p. 143.

249 Kasting, J.F., and Walker, J.C.G., 1981, Limits on oxygen concentration in the prebiological
250 atmosphere and the rate of abiotic fixation of nitrogen: *Journal of Geophysical Research*, v.
251 86, p. 1147-1158.

252 Kumar, A., Venkatesh, A.S., Ramesh Babu, P.V.R., and Nayak, S., 2012, Genetic implications of rare
253 uraninite and pyrite in quartz-pebble conglomerates from Sundargarh District of Orissa,
254 Eastern India: *Journal of the Geological Society of India*, v. 79, p. 279-286.

255 Langmuir, D. 1997, *Aqueous environmental geochemistry*. Prentice Hall, NJ, 600p.

256 Lyons, T.W., Reinhard, C.T., and Planavsky, N.J., 2014, The rise of oxygen in Earth's early ocean and
257 atmosphere: *Nature*, v. 506, p. 307-315.

258 Macfarlane A.W., Danielson, A., and Holland, H.D., 1994, Geology and major and trace element
259 chemistry of the late Archean weathering profiles in the Fortescue Group, Western Australia:
260 Implications for atmospheric PO₂: *Precambrian Research*, v. 65, p. 297–317.

261 Misra, S., Moitra, S., Bhattacharya, S., and Sivaraman T.V., 2000, Archean Granitoids at the contact
262 of Eastern Ghat granulite belt and Singhbhum-Orissa craton in Bhuban Rengali Sector,
263 Orissa, India: *Gondwana Research*, v. 3, p. 205-213.

264 Mukhopadhyay, J., Beukes, N.J., Armstrong, R.A., Zimmermann, U., Ghosh, G., and Medda, R.A.
265 2008, Dating the Oldest Greenstone in India: A 3.51-Ga Precise U-Pb SHRIMP Zircon Age
266 for Dacitic Lava of the Southern Iron Ore Group, Singhbhum craton: *Journal of Geology*, v.
267 116, p. 449-461.

268 Mukhopadhyay, J., Ghosh, G., Zimmermann, U., Guha, S., and Mukherjee, T., 2012, A 3.51 Ga
269 bimodal volcanics-BIF-ultramafic succession from Singhbhum Craton: implications for
270 Palaeoarchaeon geodynamic processes from the oldest greenstone succession of the Indian
271 subcontinent: *Geological Journal*, v. 47, p. 284–311.

272 Nesbitt, H. W., 1977, Mobility and fractionation of rare earth elements during weathering of a
273 granodiorite: *Nature*, v. 279, p. 206-210.

274 Nesbitt, H.W., and Markovics, G., 1997, Weathering of granodioritic crust, long-term storage of
275 elements in weathering profiles, and petrogenesis of siliciclastic sediments: *Geochimica et*
276 *Cosmochimica Acta*, v. 61, p. 1653-1670.

277 Ohmoto H., Watanabe Y., and Kazumasa K., 2004, Evidence from massive siderite beds for a CO₂-
278 rich atmosphere before ~1.8 billion years ago: *Nature*, v. 429, p. 395-399.

279 Ohmoto, H., 1996, Evidence in pre-2.2 Ga paleosols for the early evolution of atmospheric oxygen
280 and terrestrial biota: *Geology*, v. 24, p. 1135-1138.

281 Philippot, P., Teitler, Y., Gérard, M., Cartigny, P., Muller, E., Assayag, N., Le Hir, G., and Fluteau, F.
282 2013, Isotopic and Mineralogical Evidence for Atmospheric Oxygenation in 2.76 Ga Old
283 Paleosols: *Mineralogical Magazine*, v. 77, p. 1965.

284 Planavsky, N.J., Asael, D., Hofmann, A., Reinhard, C.T., Lalonde, S.V., Knudsen, A., Wang, X.,
285 Ossa Ossa, F., Pecoits, E., Smith, A.J.B., Beukes, N.J., Bekker, A., Johnson, T.M.,
286 Konhauser, K.O., Lyons, T.W., and Rouxel, O.J., 2014, Evidence for oxygenic
287 photosynthesis half a billion years before the Great Oxidation Event: *Nature Geoscience*, 7, p.
288 283-286.

289 Rosing, M.T., and Frei, R., 2004, U-rich Archaean sea-floor sediments from Greenland - indications
290 of > 3700 Ma oxygenic photosynthesis: *Earth and Planetary Science Letters*, v. 217, p. 237-
291 244.

292 Rye, R., and Holland, H.D., 1998, Paleosols and the evolution of atmospheric oxygen: A critical
293 review: *American Journal of Science*, v. 298, p. 621–672.

294 Tait, J., Zimmermann, U., Miyazaki, T., Presnyakov, S., Chang, Q., Mukhopadhyay, J., and Sergeev,
295 S., 2011, Possible juvenile Palaeoarchean TTG magmatism in eastern India and its
296 constraints for the evolution of the Singhbhum craton: *Geological Magazine*, v. 148, p. 340 -
297 347.

298 Xiong, J., Fischer, W.M., Inoue, K., Nakahara, M., and Bauer, C.E. 2000, Molecular Evidence for the
299 early evolution of photosynthesis: *Science*, v. 289, p. 1724-1730.

300 Yang, W., Holland, H.D., and Rye, R., 2002, Evidence for low or no oxygen in the late Archean
301 atmosphere from the 2.76 Ga Mt. Roe #2 paleosol, Western Australia: Part 3: *Geochimica et*
302 *Cosmochimica Acta*, v. 66, p. 3707-3718.

303 Yusoff, Z.M., Ngwenya, B.T., and Parsons, I., 2013, Mobility and fractionation of REEs during deep
304 weathering of geochemically contrasting granites in a tropical setting, Malaysia: *Chemical*
305 *Geology*, v. 349-350, p. 71-86.

306

307 **GSA Data Repository** item 2014xxx, [Tables DR1 & DR2, U-Pb Detrital zircon ages (LA-
308 ICPMS at Trinity College Dublin), and major and trace element concentrations of samples
309 from Keonjhar Paleosol profile (Analyses by ACME LAB, Canada)] are available online at
310 www.geosociety.org/pubs/ft2014.htm, or on request from editing@geosociety.org or
311 Documents Secretary, GSA, P.O. Box 9140, Boulder, CO 80301, USA. Major element
312 analyses were carried out by ICP-OES, whereas trace element and REE concentrations and
313 U-Pb isotope ratios were determined by solution mode and laser ablation ICP-MS
314 respectively.

315

316

317

318 **FIGURE CAPTIONS**

319 Figure 1A. Simplified geological map of the southern part of the Singhbhum Craton showing
320 distribution of siliciclastic sediments unconformably overlying the Keonjhar Paleosol,
321 Singhbhum Granite & Iron Ore Group greenstone. 1B. Field photograph of the paleosol
322 overlain by quartzarenite sandstone (hammer rests on uneven basal erosional surface). 1C.
323 BSEM image of detrital uraninite from quartzarenite and EDS spectrum showing uranium
324 (U), lead (Pb) and oxygen (O) peaks. 1D BSEM image showing detrital pyrite (p) and
325 uraninite (u) in quartzarenite. 1E. SEM image of pyrophyllite in the paleosol.

326

327 Figure 2A. Probability-age plot of 431 detrital zircon analyses (<10% discordant) from seven
328 quartzarenite sandstone samples overlying the Keonjhar Paleosol. The youngest zircon
329 population, indicated with an arrow, occurs at 3.02 Ga. The timing of the Great Oxygenation
330 Event (GOE) as well as ages for formation for the Mt. Roe, Nsuze and Pilbara paleosols are
331 indicated. 2B. Geochemical plots of paleosol samples. For Ti-normalized plots of paleosol
332 samples, note enrichment/depletion with respect to basement granite shown as circles at base
333 of each plot. 1C. REE composition of the Keonjhar Paleosol. Note HREE enrichment and
334 negative Ce-anomaly in the paleosol with respect to granite protolith. Comparison with Pr-
335 anomaly rules out effects of La-enrichment.

336

337

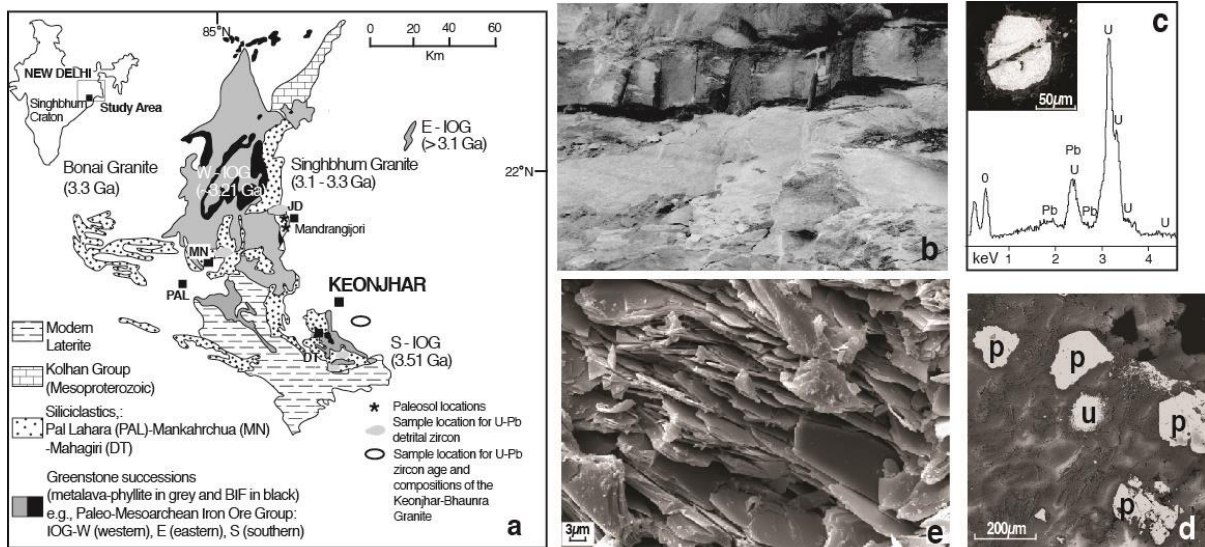
338

339

340

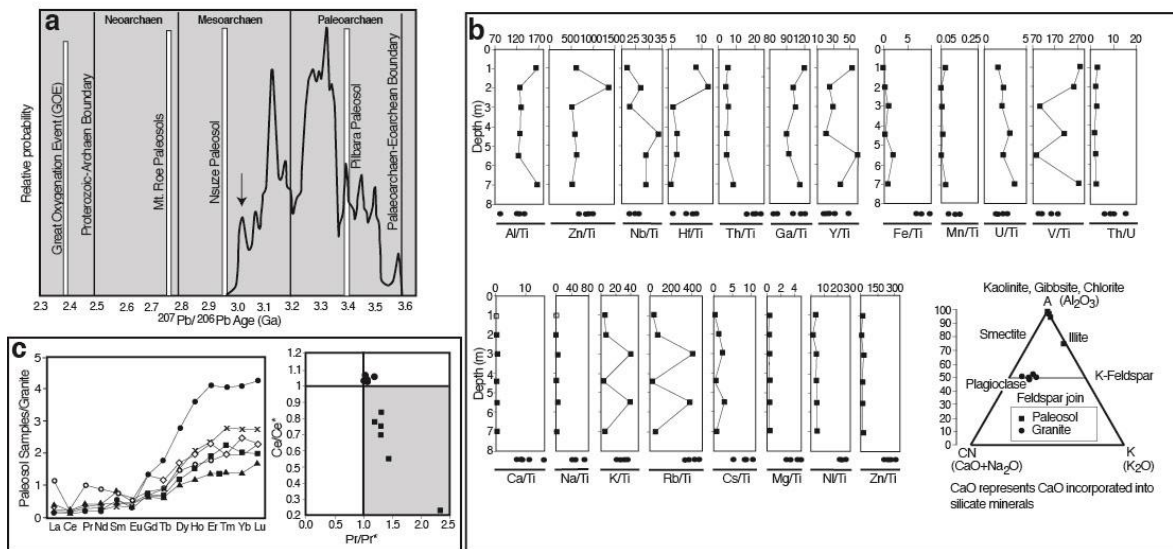
341

342 Fig. 1



343

344 Fig. 2



345

346

347 Table DR1.

348 LA-ICP-MS U-Pb detrital zircon data from quartzarenites from Mahagiri, Pal-Lahara-
349 Mankaharchua Range and from north of Keonjhar. Percentage discordance calculated as a
350 difference between $^{207}\text{Pb}/^{206}\text{Pb}$ and $^{206}\text{Pb}/^{238}\text{U}$ ages. Analyses marked * are >10% discordant
351 and are not used in construction of the probability diagram. 431 out of 770 analyses are <10%
352 discordant.

353

354 Table DR2.

355 Major (wt%) and trace element (ppm) concentrations of samples from Keonjhar Paleosol
356 profile.

357

358 **Online Section**

359 **FULL METHODS**

360 Major, trace and rare earth element analyses were carried out at the ACME Analytical
361 Laboratories (Vancouver) Ltd. Major elements were determined using a SPECTRO ARCOS
362 ICP-optical emission spectrometer (ICP-OES) following a lithium borate fusion and dilute
363 acid digestion. Loss on ignition (LOI) was determined by sintering at 1000°C and Leco
364 analysis was carried out for total carbon and sulphur. Trace element concentrations, including
365 rare earth elements (REE), were carried out using a NexION 300 ICP-MS.

366 All sandstone samples for the U-Pb zircon aspect of the study were prepared and
367 analysed at Trinity College Dublin, Ireland. Rocks were crushed, milled using a Retsch®
368 DM-200 disc mill fitted with manganese steel grinding discs, sieved to 300µm with the finer
369 grained fraction separated using a Gemini® mineral separation table, a Frantz® magnetic
370 separator (to 1.0A) and finally a methylene iodide heavy liquid separation. Following
371 mineral separation zircon from each sample was pipetted in ethanol and mounted in an epoxy

372 grain mount, ground down to expose grain interiors and polished using 6 μ m and 1 μ diamond
373 pastes. A Photon Machines Analyte Excite laser ablation system with a 30 μ m spot size was
374 used for ablations using the following settings: 28% power, repetition rate of 4Hz and 180
375 shot counts. This equates to a fluence of 3.3 J cm⁻² and an ablation pit depth of approximately
376 15 μ m. The laser ablation system was coupled to a Thermo Scientific iCAP[®] (model S)
377 quadrupole ICP-MS for isotope ratio measurements. Ablated material was transported to the
378 plasma using ultrahigh purity He which was passed through an inline Hg trap. High purity Ar
379 was employed as the plasma gas. 91500 (Wiedenbeck et al., 2004) was used as the primary
380 zircon standard to corrected for any laser or plasma induced fractionation. Both Temora
381 (Black et al., 2003) and Plešovice (Sláma et al., 2008) zircon were used as secondary
382 standards to assess accuracy and reproducibility. Typically two primary and two secondary
383 standard analyses were conducted for every 10 to 15 unknowns. Raw data were processed
384 using the VizualAge data reduction scheme (Petrus and Kamber, 2012) operating within
385 Iolite (Paton et al., 2011). Secondary standard data from several separate analytical sessions
386 give ²⁰⁶Pb/²³⁸U ages of 417.6 \pm 3.1 Ma (MSWD=5.6) for Temora-1 and 337.2 \pm 2.0 Ma
387 (MSWD=8.0) for Plešovice, which are within error of accepted values of 416.75 \pm 0.24 Ma
388 (Black et al., 2003) and 337.13 \pm 0.37 Ma (Sláma et al., 2008) respectively. All U-Pb analyses
389 reported are non-common Pb corrected. A ²⁰⁶Pb/²³⁸U versus ²⁰⁷Pb/²⁰⁶Pb age discordance was
390 calculated for all unknowns and only analyses less than 10% discordant were used in
391 construction of probability-age diagrams using Isoplot (Ludwig, 2003).

392

393 Black, L. P. et al., 2003, TEMORA 1: A new zircon standard for Phanerozoic U-Pb
394 geochronology: *Chemical Geology*, v. 200, p. 155–170.

395 Ludwig, K. R., 2003, Isoplot / Ex 3.00. A geochronological toolkit for Microsoft Excel:
396 Special Publication 4, Berkeley Geochronological Center (Berkeley, CA, USA), 70 p.

- 397 Paton, C. et al., 2011, Iolite: Freeware for the visualization and processing of mass
398 spectrometric data: *Journal of Analytical Atomic Spectroscopy*, v. 26, p. 2508–2518.
- 399 Petrus, J. A., and Kamber, B. S., 2012, VizualAge: A Novel Approach to Laser Ablation ICP-
400 MS U-Pb Geochronology Data Reduction: *Geostandards and Geoanalytical Research*,
401 v. 36, p. 247-270.
- 402 Sláma, J. et al., 2008, Plěšovice zircon – A new natural reference material for U-Pb and Hf
403 isotopic microanalysis: *Chemical Geology*, v. 249, p. 1–35.
- 404 Wiedenbeck, M., et al., 2004, Further characterization of the 91500 zircon crystal:
405 *Geostandards and Geoanalytical Research*, v. 28, p. 9–39.